

Connecting surface emissions, convective uplifting, and long-range transport of carbon monoxide in the upper troposphere: New observations from the Aura Microwave Limb Sounder

Jonathan H. Jiang,¹ Nathaniel J. Livesey,¹ Hui Su,¹ Lori Neary,² John C. McConnell,² and Nigel A. D. Richards³

Received 10 May 2007; revised 3 August 2007; accepted 24 August 2007; published 27 September 2007.

[1] Two years of observations of upper tropospheric (UT) carbon monoxide (CO) from the Aura Microwave Limb Sounder are analyzed; in combination with the CO surface emission climatology and data from the NCEP analyses. It is shown that spatial distribution, temporal variation and long-range transport of UT CO are closely related to the surface emissions, deep-convection and horizontal winds. Over the Asian monsoon region, surface emission of CO peaks in boreal spring due to high biomass burning in addition to anthropogenic emission. However, the UT CO peaks in summer when convection is strongest and surface emission of CO is dominated by anthropogenic source. The long-range transport of CO from Southeast Asia across the Pacific to North America, which occurs most frequently during boreal summer, is thus a clear imprint of Asian anthropogenic pollution influencing global air quality.

Citation: Jiang, J. H., N. J. Livesey, H. Su, L. Neary, J. C. McConnell, and N. A. D. Richards (2007), Connecting surface emissions, convective uplifting, and long-range transport of carbon monoxide in the upper troposphere: New observations from the Aura Microwave Limb Sounder, *Geophys. Res. Lett.*, **34**, L18812, doi:10.1029/2007GL030638.

1. Introduction

[2] Human activities – industrial, agricultural and residential – cause vast quantities of natural and synthetic chemicals to be emitted into the atmosphere. One of these chemicals is carbon monoxide (CO), which is mostly formed by incomplete combustion of fossil and biofuels, and by biomass burning. The total global anthropogenic CO emission is estimated at ~655 Tg/year, of which about 47% is of Asian origin [Bey *et al.*, 2001; Yevich and Logan, 2003]. Global biomass-burning emits about 485 Tg/year of CO, of which Asia contributes nearly 30% [Duncan *et al.*, 2003]. Although it is mostly emitted at the surface, CO can be rapidly uplifted into mid- and upper troposphere (UT) by convection, where it can be transported around the globe by the circulation. In addition to the emissions at surface, CO is also produced in the atmosphere through oxidation of methane and non-methane hydro-carbons by hydroxyl-radical (OH). There are two major sinks of tropospheric

CO: removal from the atmosphere through direct oxidation by OH and loss by transport to the stratosphere. The chemical lifetime of CO due to loss by OH varies between 2–8 months depending on latitude and season [e.g., Shindell *et al.*, 2006]. The timescale for transport of CO into the lower stratosphere through upwelling advection in the tropics has been estimated to be several months [e.g., Schoeberl *et al.*, 2006]. Its relatively long lifetime enables CO to be a good tracer of transport processes, such as the long-range transport of Asian pollutants across the Pacific.

[3] A number of recent field observations have documented that chemical composition over the Western Pacific is frequently perturbed by the pollutant outflow from south Asia [e.g., Jacob *et al.*, 2003]. There is also evidence from the surface and aircraft observations that shows the Asian pollution influences extend to North America [e.g., Bertsch *et al.*, 2004; Weiss-Penzias *et al.*, 2004]. Many studies, however, are largely based on observations at lower, mid-troposphere or tropospheric column. Global observations that target at the UT are limited, where the distribution and variation of CO could be much different from the lower layers [e.g., Liang *et al.*, 2004]. The Microwave Limb Sounder (MLS) instrument [Waters *et al.*, 2006] on the Aura satellite has been measuring upper tropospheric CO mixing ratios (in ppbv) since August 2004. Analysis of the MLS CO data has led to several important scientific discoveries [e.g., Li *et al.*, 2005; Fu *et al.*, 2006; Schoeberl *et al.*, 2006]. In this paper, MLS V1.5 CO data are used. The data have been screened to make sure they are not affected by clouds. The accuracy of the CO is estimated at ~30% or less for pressures 147 hPa or less. At 215 hPa, there is a persistent factor of ~2 high bias, but the morphology is validated to be realistic (N. J. Livesey *et al.*, Validation of Aura Microwave Limb Sounder O3 and CO observations in the upper troposphere and lower stratosphere, submitted to *Journal of Geophysical Research*, 2007).

[4] From time to time episodic transport events are observed by MLS. Figure 1 illustrates an example of one such transport event. The MLS observed CO averaged for 1–6 June 2006 at three UT pressure levels are shown, along with horizontal wind vectors at the same levels from the NCEP analyses. Two features in the CO distribution are clearly visible: the spatial patterns vary with height; and a CO plume extends from South Asia across the Pacific reaching the west coast of United States at 215 hPa. At 100 hPa, the enhanced CO is mostly concentrated over the Tibetan Plateau due to a strong “trapping effect” of the Asian summer monsoon anticyclone [Li *et al.*, 2005]; At 147 hPa, the CO enhancements extend eastward to the

¹Jet Propulsion Laboratory, California Institute of Technology, Pasadena, California, USA.

²Department of Earth and Space Science and Engineering, York University, Toronto, Ontario, Canada.

³Institute for Atmospheric Science, University of Leeds, Leeds, UK.

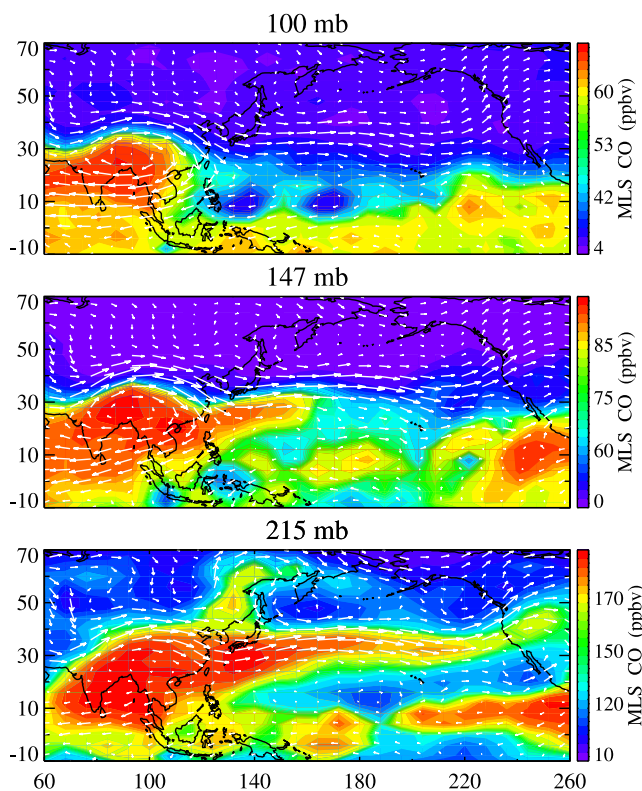


Figure 1. MLS measured CO mean mixing ratios for 1–6 June 2006 at three upper tropospheric pressure levels. The white arrows are the mean NCEP vector winds (U, V) at the same pressure levels. The data are averaged on $8^\circ \times 4^\circ$ longitude by latitude grids.

middle North Pacific; At 215 hPa, a clear outflow of CO rich air is observed to emanate from South Asia, following the mid-latitude westerly jet across the North Pacific and eventually penetrating the western United States. Such CO enhancements and long-range transport events are observed sporadically ~ 5 times or more per year in the MLS observations.

[5] In this paper, we use two-year (2004–2006) MLS CO observations, CO emission climatology, MLS cloud ice water content (IWC, V1.5), as well as outgoing longwave radiation (OLR) and winds from the NCEP analyses to estimate the impact of surface emission, convection and tropospheric winds on the distribution and variation of CO in the UT, with a focus on the Southeast Asia and North Pacific regions. The seasonal variability of long-range transport of Asian pollutants across North Pacific will be highlighted.

2. Surface Emissions

[6] We first examine the surface emissions of CO: their spatial distribution, seasonal changes and how CO may disperse immediately after release. In Figures 2a and 2b, the color shading shows the surface fluxes of CO from biomass-burning and anthropogenic sources, respectively. The biomass-burning emissions (Figure 2a) are from the climatological inventory described by *Duncan et al.* [2003]. Biomass burning has a strong seasonal variation, which

oscillates from the northern to the southern sub-tropics over the course of a year. From October to April when the tropical rain belt associated with the Intertropical Convergence Zone (ITCZ) lies mostly in the southern hemisphere, the northern sub-tropics are under the influence of the descending branch of the Hadley cell and experience mostly dry conditions. Hence, forest fires frequently occur over the South Asia landmass, especially during second half of this “dry” period (in winter and spring). From May to September, the ITCZ lies in the northern hemisphere and is accompanied by active monsoonal rainfall, which suppresses biomass burning during this “wet” period. The anthropogenic emissions shown are from climatology inventory described by *Bey et al.* [2001] and *Yevich and Logan* [2003], which consists of mainly fossil fuel (e.g. coal-fired power plants) and biofuel combustion. These anthropogenic emissions are located at human population centers and are relatively stable with little seasonal variations (Figure 2b).

[7] To illustrate how the CO-loaded air may be dispersed and transported after being released from the source region, sea-level-pressure (SLP) and near-surface (700 hPa) horizontal winds from NCEP analyses are over-plotted in Figures 2a and 2b, respectively. Low SLP indicates the regions of convergence and ascent, whereas high SLP shows region of divergence and subsidence. The near-surface winds give an indication of the direction in which the emitted CO could disperse in the boundary layer and lower troposphere. In January, strong north-westerlies would lead to transport of the Asian anthropogenic CO to North Pacific in the lower troposphere (see wind contours in Figure 2b, Jan06), but it is unlikely to be lifted up to the UT because of the strong subsidence over Asia, indicated by the high SLP contours in Figure 2a (Jan06). In July, the westerly winds are the weakest compared to other seasons and are located further north between 30°N and 50°N . There is also strong ascent associated with the Asian summer monsoon convection that can loft CO into the mid-troposphere and UT. Spring and fall seasons represent transition periods where the mid-latitude westerlies are stronger than those of summer but convection over Asia is modest. In April, eastward winds occur throughout latitudes between 10°N and 50°N with moderate ascending air at equatorial South Asia, favoring upward transport of Asian CO. In the fall, the eastward winds are located further north at latitudes poleward of 30°N , far away from the tropical convection zone, a condition under which the vertical transport of CO may be limited.

3. Deep Convection

[8] Deep convection is a process that can cause rapid injection of boundary layer CO into the UT. Figure 2c shows the MLS observed IWC, over-plotted with NCEP 240 W/m^2 OLR contour. Regions with large MLS IWC are generally collocated with regions of low OLR, so that we can use IWC as a good indicator of deep-convection [*Su et al.*, 2006]. The strength and location of deep convection (shown by large IWC) vary considerably from season to season. From winter to summer, the maximum of the tropical convection migrates northward from the Western Pacific to South and Southeast Asian. During summer, strong convection is associated with Asian summer

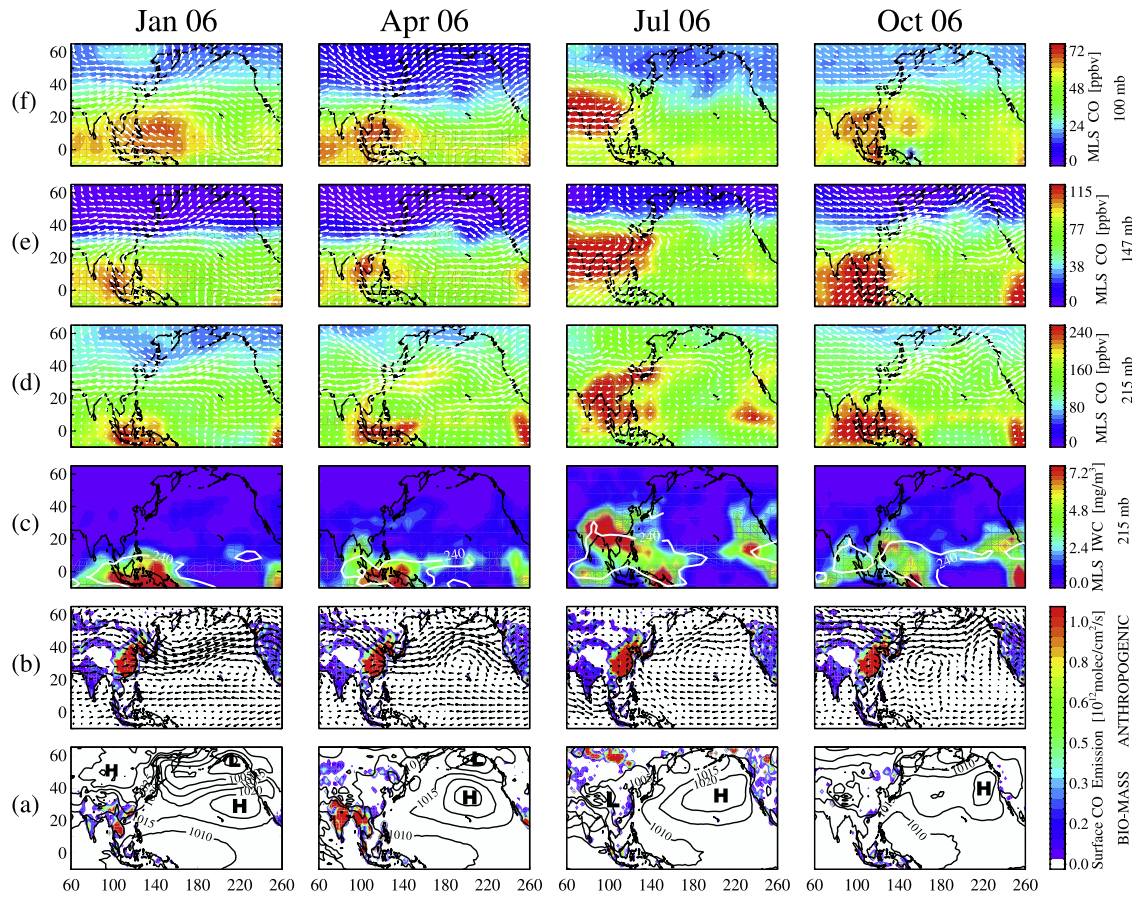


Figure 2. From left to right columns are monthly mean values (January, April, July, October 2006) averaged on $8^\circ \times 4^\circ$ longitude by latitude grids. (a) Bio-mass burning emissions of CO (color-filled contour) and NCEP sea-level-pressure (line contour). (b) Anthropogenic CO emissions (color-filled contour) and the 900 hPa vector winds (U,V) from NCEP analysis. (c) MLS measured IWC at 215 hPa and the 240 W/m^2 OLR contours in white line contours for the tropical region from NCEP (low OLR in the high-latitude are not shown). (d, e, f) MLS measured CO mixing ratios at 215 hPa, 147 hPa, and 100 hPa pressure levels, respectively, over plotted by NCEP vector winds at same pressures levels.

monsoon (ASM) with the largest IWC at northern subtropics over the landmass of North India, South and Southeast China. The summer-time winds over those regions are characterized by a strong convergence at the lower troposphere and a divergence in the UT (South Asian anticyclone-SAA). The associated monsoon circulation and deep convection result in rapid vertical transport of polluted boundary layer air in this region. This convective pattern usually starts in late spring and lasts throughout summer until the convective activity retreats southward to the ocean in mid-fall.

4. Upper Tropospheric CO

[9] Figures 2d, 2e, and 2f show monthly means of MLS measured CO at three UT pressure levels over-plotted with the NCEP horizontal winds at the same height and during the same period. Clearly there is a high degree of seasonal variability in UT CO. In January, even though there is biomass burning emission in South Asia, no significant amount of CO are lifted in to the UT because the convective activity is located farther south in the maritime continent. In April, the convection pattern shifts northward, partially overlapping with the Southern Asia biomass burning region.

However, the center of deep convection is still located further south, resulting in only moderate CO enhancement in the UT over Southern Asia. Outflow of CO from Southern Asia can be seen at 215 and 147 hPa pressure levels, indicating transport of upper tropospheric air into North Pacific. In July, heavy precipitation extinguishes most of the biomass burning in South Asia region. At the same time, deep convection over land associated with the ASM carries large amount of anthropogenically polluted boundary layer air into the UT, resulting in high concentrations of CO over South Asia. The SAA is located over the Tibetan Plateau, with strong northeasterly winds on the southern flank of the Plateau. At 147 to 100 hPa, elevated concentrations of CO are observed over India and across central and eastern China, where the upper level anticyclone prevails. Enhanced CO concentrations also extend from Southeast Asia to the Arabian Sea, transported by the strong easterly winds to the south of the SAA. The CO observations from MLS are broadly consistent with the large-scale wind patterns (Figures 2e and 2f, July 06). At 215 hPa (Figure 2d, July 06), the anticyclonic flow is weaker than that at upper levels. Substantial CO enhancement in the Pacific can be seen at this altitude, indicating long-range transport of CO rich air by westerly winds. Further north in

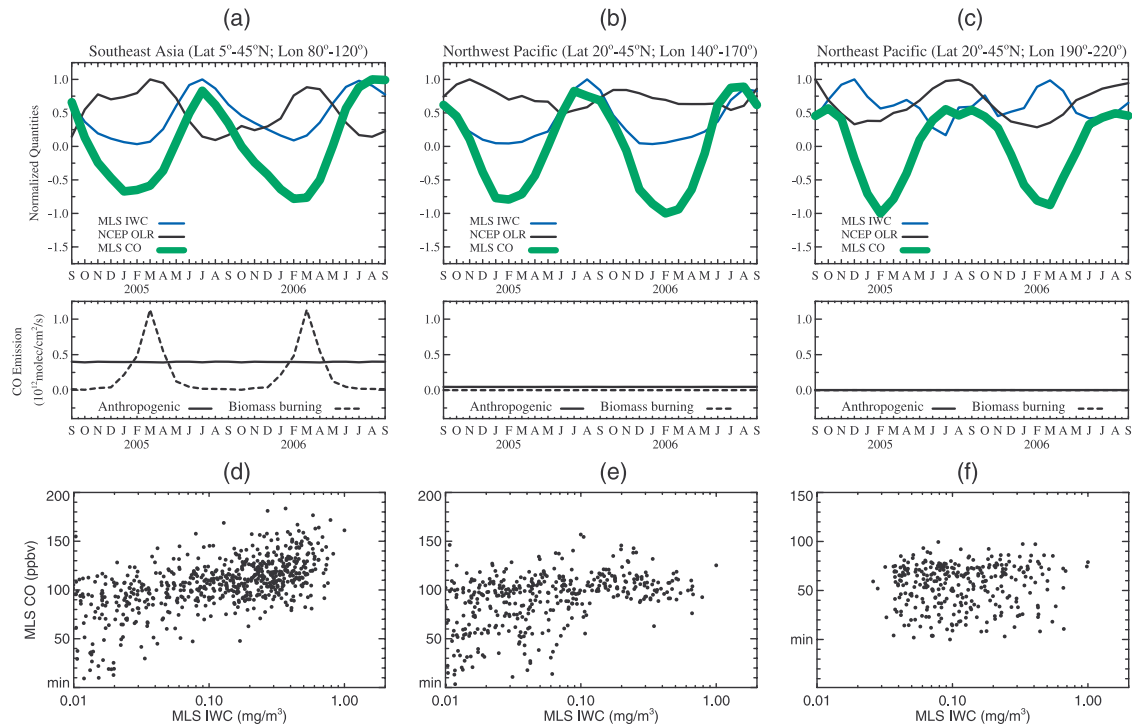


Figure 3. (top) Time evolution of monthly mean 147 hPa MLS CO anomaly (thick green line), 147 hPa MLS IWC (blue line), and NCEP OLR above 240 W/m² (black line). (middle) Time evolution of monthly mean CO emissions from biomass burning (dashed line) and anthropogenic (solid line) sources. (bottom) Scatter plots of MLS CO versus IWCs at 147 hPa. From left to right, for regions of Southeast Asia, Northwest Pacific, and Northeast Pacific. All data are 8° × 4° longitude by latitude gridded averages. The scatter plots consists of 25 monthly mean data from September 2004 to September 2006.

Eurasia (~60°N, Figure 2a), there is bio-mass burning but its influence on UT CO is limited due to the weak convection in that region. The amount of upper tropospheric CO in the fall season is lower than that in summer, but somewhat higher than those in spring and winter.

5. Seasonality of Long-Range Transport

[10] Figure 3 shows the seasonal variation of UT CO and its connection with deep convection and surface emission sources. We consider three separate regions: Southeast Asia (SEA), which contains most of the emission sources; the Northwest Pacific (NWP), located downwind from the emission sources, offshore of China; and the Northeast Pacific (NEP), which is further down-stream close to the North American coast. The upper panels in Figure 3 illustrate the monthly mean quantities of MLS measured CO anomaly and IWC, both at 147 hPa, and NCEP OLR minus 240 W/m². All quantities are normalized so that the maximum absolute value is 1. The CO anomaly refers to the departure of monthly mean CO from its 2-year mean. The lower panels are the monthly mean CO emissions from the biomass burning and anthropogenic sources. We choose our analysis at 147 hPa because the MLS data have better quality at 147 hPa than at 215 hPa.

[11] The seasonal variability in UT CO over the SEA closely follows the seasonal cycle of deep-convection indicated by OLR and IWC. The upper panel of Figure 3a shows that the CO over the Southeast Asia reaches the maximum in the mid-summer (July), when the convection is

the strongest. The biomass burning in SEA peaks in March but is smallest in summer and fall (see lower panel of Figure 3a). Therefore the maximum UT CO loading in summer months above SEA is mostly from the anthropogenic emissions, which are almost constant throughout the year. The scatter plot between the observed CO and IWC in Figure 3d shows a clear positive correlation between the observed CO and IWC, with a correlation coefficient of 0.6, indicating a convective transport of CO rich air in the UT.

[12] In the NWP, there is little CO emission over the ocean surface, except from some scattered islands. Also there is smaller variation of convection in NWP compared to that in SEA, indicated by the smaller changes in OLR. Nevertheless, a weaker but still positive correlation exists between the CO and IWC (Figure 3e) at 147 hPa with correlation factor of 0.3, and the seasonal variation of CO occurs at the same phase as IWC - peaks in summer and dips in winter (Figure 3b). This may suggest that the outflow of CO rich air and the detrainment of cirrus clouds are from the same source region of SEA and are transported by westerly winds.

[13] Over the NEP, there is neither biomass burning nor anthropogenic emission source. The variation of CO is not correlated with local convection as illustrated both by the time-series (Figure 3c) and by the scatter plot (Figure 3f). The correlation coefficient between the CO and IWC is less than 0.07. The seasonal variation of CO there is thus likely controlled by the long-range transport from SEA. It is also interesting to see that in NEP, the CO maximum becomes broader - it lasts longer into September, 2 months after

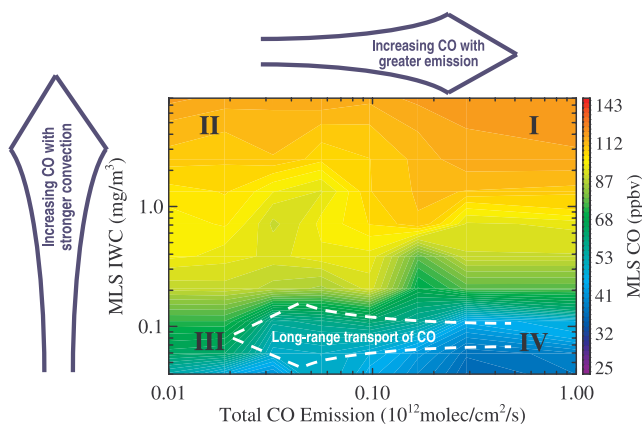


Figure 4. Contour plots of MLS CO mixing ratio at 147 hPa binned according to the total surface emission and MLS IWC amount at same pressure. All data are monthly mean values from September 2004 to September 2006 on $8^\circ \times 4^\circ$ longitude by latitude grids.

peak CO in SEA. We note that September is the peak biomass burning season in South America. Our analyses (not shown here) indicate the apparent longer lasting CO peak in NEP, compared to that in SEA and NWP, is likely due to easterly and southeasterly transport of CO from biomass burning in South America.

6. Conclusion

[14] The relationship between surface emission, deep convection and long-range transport and their impact on the UT CO loadings can be summarized in Figure 4, in which the monthly mean MLS CO mixing ratios at 147 hPa gridded on the 8° (longitude) \times 4° (latitude) grid-boxes in the northern hemisphere (0° – 60° N) from September 2004 to September 2006 are binned according to the total (anthropogenic and biomass burning) CO surface emissions (x-axis) and the MLS IWC (y-axis). In general, the CO mixing ratio is high when convection is strong, indicated by the ascending arrow to the left of the y-axis. With the presence of deep convection, CO concentration roughly increases with increasing surface emission (see the arrow above Figure 4). When deep convection is absent, the UT CO is generally low and bears little connection with surface emissions. Thus the variation of the UT CO may result from long-range transport, as indicated by the dashed arrow near the x-axis. Interestingly, the 4 corners in Figure 4 represent four typical regimes of CO variability in the UT, each of which bears a distinct character of the relations among surface emission, deep convection, and horizontal transport of CO.

[15] Regime I. Both surface emission and convection are strong; the maximum UT CO concentrations in this regime result from vigorous convective deposition of surface emission. SEA in summer is a typical Regime I, where strong deep convection is coupled with anthropogenic emission.

[16] Regime II. There is strong convection but very little surface emission; the high CO in this regime may come from transport at the same height or from the convective lifting of lower level CO that transported from other source

regions. The NWP region shown in Figure 3b shows some characteristics of this regime. On daily basis, there are also regions with low CO concentration and zero surface emission but considerable convection, which are not shown in Figure 4 (Note the log-scale x-axis does not start at zero).

[17] Regime III. There is no convection and no surface emission; the CO enhancements in this regime may indicate long-range transport of CO rich air from other regions at same altitude. The NEP shown in Figure 3c belongs to this category.

[18] Regime IV. The surface emissions are strong but no convection is present so that a relatively small fraction of emissions make it to the 147 hPa level. The lack of CO enhancement in this regime means that horizontal transport of CO is also limited. For example, the Eurasia region in July 06 (Figure 2a, Jul 06) experienced a strong bio-mass burning, but no CO enhancement (Figure 2e), due to lack of deep convection and horizontal transport.

[19] Based on MLS CO observations, the highest CO concentrations in the northern hemisphere UT occur in summer when deep convection reaches peak intensity. At that time, the surface emission of CO is dominated by anthropogenic source. During winter and spring, the CO concentration in the UT is relatively weak despite of strong biomass-burning events, mainly due to the lack of deep convection directly over the emission source. The UT CO observed by MLS thus includes a clear imprint of Asian anthropogenic pollution in the global circulation and air quality.

[20] **Acknowledgments.** This work was conducted at the Jet Propulsion Laboratory, California Institute of Technology, supported by NASA. JHJ and HS thank Phil DeCola and the NASA Atmospheric Composition program NNH05ZDA001N for support. LN and JCM wish to thank the Canadian Foundation for Climate and Atmospheric Science for support via MAQNet grant. We also acknowledge the support from Aura Project, and wish to thank useful comments from M. Schoeberl, S. Massie, C. Liu, Q. Li, J. Waters, and M. Santee.

References

- Bertschi, I. T., D. A. Jaffe, L. Jaeglé, H. U. Price, and J. B. Dennison (2004), PHOBEA/ITCT 2002 airborne observations of transpacific transport of ozone, CO, volatile organic compounds, and aerosols to the north-east Pacific: Impacts of Asian anthropogenic and Siberian boreal fire emissions, *J. Geophys. Res.*, **109**, D23S12, doi:10.1029/2003JD004328.
- Bey, I., D. J. Jacob, J. A. Logan, and R. M. Yantosca (2001), Asian chemical outflow to the Pacific in spring: Origins, pathways, and budgets, *J. Geophys. Res.*, **106**(D19), 23,097–23,114, doi:10.1029/2001JD000806.
- Duncan, B. N., R. V. Martin, A. C. Staudt, R. Yevich, and J. A. Logan (2003), Interannual and seasonal variability of biomass burning emissions constrained by satellite observations, *J. Geophys. Res.*, **108**(D12), 4100, doi:10.1029/2002JD002378.
- Fu, R., et al. (2006), Short circuit of water vapor and polluted air to the global stratosphere by convective transport over the Tibetan Plateau, *Proc. Nat. Acad. Sci. U. S. A.*, **103**, 5664–5669.
- Jacob, D. J., J. H. Crawford, M. M. Kleb, V. S. Connors, R. J. Bendura, J. L. Raper, G. W. Sachse, J. C. Gille, L. Emmons, and C. L. Heald (2003), Transport and Chemical Evolution over the Pacific (TRACE-P) aircraft mission: Design, execution, and first results, *J. Geophys. Res.*, **108**(D20), 9000, doi:10.1029/2002JD003276.
- Li, Q., et al. (2005), Convective outflow of South Asian pollution: A global CTM simulation compared with EOS MLS observations, *Geophys. Res. Lett.*, **32**, L14826, doi:10.1029/2005GL022762.
- Liang, Q., L. Jaeglé, D. A. Jaffe, P. Weiss-Penzias, A. Heckman, and J. A. Snow (2004), Long-range transport of Asian pollution to the northeast Pacific: Seasonal variations and transport pathways of carbon monoxide, *J. Geophys. Res.*, **109**, D23S07, doi:10.1029/2003JD004402.
- Schoeberl, M. R., B. N. Duncan, A. R. Douglass, J. Waters, N. Livesey, W. Read, and M. Filipiak (2006), The carbon monoxide tape recorder, *Geophys. Res. Lett.*, **33**, L12811, doi:10.1029/2006GL026178.

- Shindell, D. T., et al. (2006), Multimodel simulations of carbon monoxide: Comparison with observations and projected near-future changes, *J. Geophys. Res.*, *111*, D19306, doi:10.1029/2006JD007100.
- Su, H., W. G. Read, J. H. Jiang, J. W. Waters, D. L. Wu, and E. J. Fetzer (2006), Enhanced positive water vapor feedback associated with tropical deep convection: New evidence from Aura MLS, *Geophys. Res. Lett.*, *33*, L05709, doi:10.1029/2005GL025505.
- Waters, J. W., et al. (2006), The Earth Observing System Microwave Limb Sounder (EOS MLS) on the Aura satellite, *IEEE Trans. Geosci. Remote Sens.*, *44*, 1075–1092.
- Weiss-Penzias, P., D. A. Jaffe, L. Jaeglé, and Q. Liang (2004), Influence of long-range-transported pollution on the annual and diurnal cycles of carbon monoxide and ozone at Cheeka Peak Observatory, *J. Geophys. Res.*, *109*, D23S14, doi:10.1029/2004JD004505.
- Yevich, R., and J. A. Logan (2003), An assessment of biofuel use and burning of agricultural waste in the developing world, *Global Biogeochem. Cycles*, *17*(4), 1095, doi:10.1029/2002GB001952.
-
- J. H. Jiang, N. J. Livesey, and H. Su, Jet Propulsion Laboratory, California Institute of Technology, Mail Stop 183-701, 4800 Oak Grove Drive, Pasadena, CA 91109-8099, USA. (jonathan.h.jiang@jpl.nasa.gov)
- J. C. McConnell and L. Neary, Department of Earth and Space Science and Engineering, York University, 113 Petrie Building, 4700 Keele Street, Toronto, ON, Canada M3J 1P3.
- N. A. D. Richards, Institute for Atmospheric Science, University of Leeds, Leeds LS2 9JT, UK.